Resonant photoionization of singly charged sulfur

S. S. Tayal*
Department of Physics, Clark Atlanta University, Atlanta, Georgia 30314, USA
(Received 13 April 2006; published 2 August 2006)

Resonance structures in the photoionization of S^+ for the removal of a $3p$ or $3s$ electron from the ground $3s^2 3p^3\ ^4S^o$ and excited metastable $^2D^o$ and $^2P^o$ states have been studied in the *B*-spline *R*-matrix approach. The nonorthogonal orbitals have been used for an accurate representation of the initial S^+ bound states, the final S^{2+} ion plus photoelectron states and S^{2+} thresholds. Calculations have been carried out in 17- and 27-state close-coupling approximations. The relativistic effects have been incorporated in the Breit-Pauli Hamiltonian. Photoionization cross sections are dominated by $3s^2 3p^2(^1D)ns\ ^2D$, $3s^2 3p^2(^1D)nd\ ^2F$, ^2D, ^2P, and $3s3p^3(^5S^o$, $^3S^o$, $^3D^o$, $^3P^o)np\ ^4P$ Rydberg series of autoionizing resonances. The resonance states are identified and analyzed to obtain resonance positions E_r, effective quantum numbers n^*, and widths Γ_r using a procedure of eigenphase gradients. The resonance line shape and correlation parameters have also been determined. Photoionization cross sections have been calculated in both length and velocity formulations that exhibit very good agreement (within 5%) with each other for most photon energies. Our results are compared with a recent merged ion-photon beam experiment. Significant discrepancies between the theoretically predicted and experimentally measured resonance structures and continuum cross sections are noted.

DOI: 10.1103/PhysRevA.74.022704 PACS number(s): 32.80.Fb, 32.80.Dz

I. INTRODUCTION

Photoionization studies of open-shell atoms and ions are of great theoretical and experimental interest because of the importance of electron correlation and interchannel coupling effects. The correlation among the electrons plays an important role in the determination of structure and dynamics of atomic systems. In addition to intrinsic physical interest, accurate photoionization cross sections of ions of astrophysical interest are needed to model a wide range of objects such as planetary nebulae, H II regions, active galactic nuclei, novae, and supernovae. A number of strong features due to sulfur ions have been observed in the spectra of the Io plasma torus [1] and of the Sun and stellar transition regions [2]. The absolute photoionization cross sections of singly charged sulfur have recently been measured in a merged ion-photon beam experiment using synchrotron-radiation from an undulator [3]. The synchrotron-radiation beam from an undulator provides much higher photon flux than the radiation from a bending magnet. The measured absolute photoionization cross sections show significant discrepancies with the previously available calculated results from the opacity project (OP) (http://heasarc.gsfc.nasa.gov/topbase/topbase.html). The OP calculations have been performed in *LS*-coupling *R*-matrix approximation [4]. In an effort to resolve the existing discrepancies between theory and experiment, we report on the photoionization cross sections of S^+ across autoionizing series of resonances converging to several S^{2+} thresholds. Theoretical calculations have been improved by using better representation of S^+ initial bound and final S^{2+} plus electron continuum states and by including a larger set of residual S^{2+} states in the close-coupling expansion within the framework of the *B*-spline *R*-matrix approach [5,6]. In addition to nonrelativistic *R*-matrix calculations, we have performed a Breit-Pauli *R*-matrix calculation to investigate the importance of relativistic effects and to check the additional Rydberg series of resonances allowed due to the inclusion of spin-orbit interaction.

The dominant resonance structures in photoionization cross sections from the $S^+\ 3s^2 3p^3\ ^4S^o$ ground state are mostly due to autoionizing Rydberg series converging to the S^{2+} $3s3p^3\ ^5S^o$, $^3S^o$, $^3D^o$, and $^3P^o$ thresholds and are caused by the photoexcitation of a $3s$ electron. The resonance structures in the photoionization cross section in the photon energy region between 20.30 and 23.34 eV are due to photoionization from the $S^+\ 3s^2 3p^3\ ^2D^o$ and $^2P^o$ metastable states. The photoionization of a $3p$ or $3s$ electron from the S^+ initial ground configuration terms $3s^2 3p^3\ ^4S^o$, $^2D^o$, and $^2P^o$ gives rise to S^{2+} $3s^2 3p^2\ ^3P$, ^1D, ^1S or $3s3p^3\ ^5S^o$, $^3D^o$, $^3P^o$, $^3S^o$, $^1D^o$, $^1P^o$ states. The inclusion of S^{2+} states such as $3s^2 3p3d\ ^3D^o$, $^3P^o$, $^3F^o$, $^1D^o$, $^1P^o$, $^1F^o$, $3s^2 3p4s\ ^3P^o$, $^1P^o$, $3s^2 3p4p\ ^1P$, ^3D, ^3S, $3s^2 3p4d\ ^3D^o$, $^3P^o$, $^3F^o$, and $^1D^o$ allows for the photoionization process where one electron is ejected and a second electron is promoted to an excited state. We have performed fairly extensive nonrelativistic and Breit-Pauli *R*-matrix calculations for the photoionization cross sections by including 17 and 27 residual S^{2+} terms in the close-coupling expansion. Our calculations have been carried out across all the autoionizing Rydberg series of resonances converging to these ionic thresholds at a fine energy mesh. We have attempted to obtain an accurate description of electron correlations both in the initial and final states in a consistent manner by *B*-spline *R*-matrix basis functions. No orthogonality constraint has been imposed on the bound and continuum functions. The completeness of the *B*-spline basis ensures that no Buttle correction to the *R*-matrix elements is required. The positions E_r, effective quantum numbers n^*, widths Γ_r, and shape parameters of the major resonances are reported. The shape parameters describing Fano profiles [7,8] can provide important information on the dynamics of excited atoms.

*Electronic address: stayal@cau.edu

 ©2006 The American Physical Society

II. THEORETICAL DETAILS

A. Wave functions for S^{2+} thresholds

Accurate description of S^{2+} residual ionic states and the S^{+} initial and final states is an important component of a reliable photoionization calculation. First we present a description of electron correlations in the representation of S^{2+} thresholds. Each of the 27 S^{2+} states considered in our work is described by fairly extensive configuration-interaction (CI) wave functions. The states of the $3s3p^3$ configuration show strong mixing with states of the $3s^23p3d$ configuration with the same symmetry. For example, $3s3p^3\ ^3P^o$ and $3s^23p3d\ ^3P^o$ states and $3s3p^3\ ^1P^o$ and $3s^23p3d\ ^1P^o$states interact very strongly. It is essential that the wave functions represent these interactions properly to obtain an accurate description of S^{2+} thresholds. The wave functions for S^{2+} show strong term dependence of the one-electron orbitals and large correlation corrections. The term-dependent nonorthogonal orbitals in the multiconfiguration Hartree-Fock approach [9,10] have been used to provide an adequate treatment of large correlation corrections and the strong interactions between the $3s^23pnd$ Rydberg series and $3s3p^3$ perturber states.

The nonorthogonal orbitals are obtained by separate optimization of different S^{2+} states. First the $1s$, $2s$, $2p$, $3s$, and $3p$ orbitals are obtained in a Hartree-Fock calculation on the $3s^23p^2\ ^3P$ state. The $3s$ and $3p$ orbitals in the $3s^23p^2$, $3s3p^3$, and $3s^23pnl$ configurations differ, and these are also different for states of different symmetries. Thus to account for term dependence of orbitals we generated several sets of $3s$ and $3p$ orbitals. Different valence $3d$, $4d$, $4s$, and $4p$ orbitals are obtained for the individual $3s^23pnl\ ^{1,3}L$ (L=0,1,2,3) states in separate calculations. Additional to spectroscopic orbitals we obtained three sets of s, p, d, and f orbitals to account for core correlation, core-polarization or core-valence correlation and interactions between different Rydberg series and perturbers (sp^3-s^2pd interactions). The mean radii of the correlation orbitals are comparable to the spectroscopic orbitals and thus represent the correlation corrections very well.

The states of the $^3P^o$, $^3D^o$, $^1P^o$, and $^1D^o$ symmetries belonging to the $3s3p^3$ and $3s^23p3d$ configurations exhibit low purity because of the strong sp^3-s^2pd interactions. The situation for the states of $^3P^o$ symmetries is most complex because of the strong mixing of the $3s^23p3d\ ^3P^o$ and $3s^23p4s\ ^3P^o$ states as well. These two states interact strongly with each other partly because of their closeness. The interaction between these two states is so strong that it is very difficult to identify these states unambiguously based on their dominant eigenvector. Following is the composition of $^3P^o$ states in our calculation:

$$3s3p^3\ ^3P^o: -0.8886(3s3p^3) - 0.4098(3s^23p3d) - 0.0334(3s^23p4s);$$

$$3s^23p3d\ ^3P^o: -0.6421(3s^23p3d) - 0.6462(3s^23p4s) + 0.3185(3s3p^3);$$

$$3s^23p4s\ ^3P^o: -0.7199(3s^23p4s) + 0.5967(3s^23p3d) - 0.2426(3s3p^3).$$

We identify the second lowest $^3P^o$ state as $3s^23p4s\ ^3P^o$ based on the composition, whereas the NIST compilation [13] listed $3s^23p3d\ ^3P^o$ as the second lowest. The composition of $3s3p^3\ ^1P^o$ state is 65.9% $3s3p^3$ and 28.1% $3s^23p3d$, while for the $3s^23p3d\ ^1P^o$ state it is 60.8% $3s^23p3d$, 24.6% $3s3p^3$, and 2% $3s^23p4s$. The purity of $3s3p^3\ ^3D^o$ and $3s^23p3d\ ^3D^o$ is only 81.5% and 78.5%, respectively. The states of the $3s^23p^2$, $3s3p^3$, and $3s^23pnl$ configurations show different correlation patterns [11,12]. The CI expansions for the $3s^23p^2$ and $3s^23pnl$ states exhibit much slower convergence than the $3s3p^3$ states. The spectroscopic and correlation functions are used to construct CI expansions for various S^{2+} states by allowing one-electron and two-electron excitations from the main configurations that describe 27 *LS* terms in our calculation. Progressively larger calculations are performed in a systematic manner to make sure that the strong interactions between various Rydberg series and perturber states are properly accounted. In order to assess the quality of wave functions used for the description of S^{2+} thresholds, we have listed calculated ionization energies of the lowest 31 fine-structure levels in Table I and compared these with the experimental values from the NIST compilation (http://physics.nist.gov; [13]). Johansson *et al.* [14] reported comprehensive laboratory analysis of the S^{2+} spectra. As indicated before, our identification of the $3s^23p3d\ ^3P^o$ and $3s^23p4s\ ^3P^o$ states does not agree with experiment. The ionization energies for the S^{2+} thresholds are calculated by using calculated ionization energy of the $S^+\ 3s^23p^3\ ^4S^o$ state which will be described in the next section. The present calculation shows good agreement with experiment for most thresholds, particularly for the lower levels of the $3s^23p^2\ ^3P$, ^1D, ^1S, $3s3p^3\ ^5S^o$, $^3S^o$, $^3P^o$, $^3D^o$, $^1P^o$, and $3s^23p3d\ ^3F^o$, $^1D^o$ *LS* terms. The calculated ionization energy for the $3s3p^3\ ^5S^o$ threshold is lower than the measured value by 0.114 eV. The overall good agreement between the calculated and measured values provides us confidence that our wave functions give a good representation of the states of S^{2+} for use in *R*-matrix calculations.

Another important test of the quality of wave functions to describe electron correlations can be provided by the oscillator strengths between the S^{2+} states. The calculations of oscillator strengths for the dipole-allowed transitions in S^{2+} have been previously reported by Nahar and Pradhan [15] and by Tayal [11]. The oscillator strengths for dipole-allowed transitions are given in Table II where the present results are compared with previous extensive theoretical calculations of Nahar and Pradhan [15] and Tayal [11], and with measured values of Berry *et al.* [16], Irwin *et al.* [17], Livingston *et al.* [18], and Ryan *et al.* [19]. A good agreement between the length and velocity gauges as well as with previous calculations can be noted. This agreement suggests that our wave functions take proper account of the important correlation and relaxation effects, and CI expansions for different S^{2+} thresholds are converged. Three calculations presented in Table II have been carried out with three independent sets of widely used computer codes [4,6,10,20]. It is clear from Table II that these theoretical results have converged to very similar values of oscillator strengths. Large differences with the calculation of Nahar and Pradhan [15] for the $3s^23p^2\ ^1D$-$3s3p^3\ ^1D^o$, $3s^23p3d\ ^1D^o$ transitions are basically due to in-

TABLE I. Calculated and experimental ionization energies (eV).

Index	State	J	Theory	Experiment	Difference
1	$3s^23p^2\ ^3P$	0	23.323	23.338	0.015
2		1	23.355	23.374	0.019
3		2	23.414	23.441	0.027
4	$3s^23p^2\ ^1D$	2	24.843	24.741	–0.102
5	$3s^23p^2\ ^1S$	0	26.862	26.705	–0.157
6	$3s3p^3\ ^5S^o$	2	30.498	30.612	0.114
7	$3s3p^3\ ^3D^o$	1	33.818	33.754	–0.064
8		2	33.822	33.758	–0.064
9		3	33.829	33.764	–0.065
10	$3s3p^3\ ^3P^o$	2	35.614	35.580	–0.034
11		0	35.615	35.583	–0.032
12		1	35.615	35.584	–0.031
13	$3s^23p3d\ ^1D^o$	2	36.282	36.251	–0.031
14	$3s^23p3d\ ^3F^o$	2	38.700	38.478	–0.222
15		3	38.733	38.513	–0.220
16		4	38.777	38.562	–0.215
17	$3s3p^3\ ^1P^o$	1	40.532	40.304	–0.228
18	$3s3p^3\ ^3S^o$	1	40.651	40.455	–0.196
19	$3s^23p4s\ ^3P^o$	0	41.336	41.079	–0.257
20		1	41.355	41.082	–0.273
21		2	41.392	41.083	–0.309
22	$3s^23p3d\ ^3P^o$	1	41.867	41.530	–0.337
23		0	41.877	41.525	–0.352
24		2	41.883	41.655	–0.228
25	$3s^23p4s\ ^1P^o$	1	41.955	41.736	–0.219
26	$3s^23p3d\ ^3D^o$	1	42.094	41.631	–0.463
27		2	42.108	41.649	–0.459
28		3	42.119	41.655	–0.464
29	$3s3p^3\ ^1D^o$	2	42.673	42.180	–0.493
30	$3s^23p3d\ ^1F^o$	3	43.338	42.878	–0.460
31	$3s^23p3d\ ^1P^o$	1	44.220	43.688	–0.532

terchange of the two $^1D^o$ states in their calculation. Our results are in excellent agreement with the measured values of Berry *et al.* [16] and Livingston *et al.* [18] for the resonance $3s^23p^2\ ^3P$-$3s3p^3\ ^3D^o$ transition and with the experiment of Irwin *et al.* [17] for the $3s^23p^2\ ^1D$ - $3s3p^3\ ^1D^o$ transition. However, there is a large discrepancy with the experiment of Berry *et al.* [16] for the latter transition, perhaps caused by the misidentification of the $3s3p^3\ ^1D^o$ state in the experiment. All three calculations show excellent agreement with each other for the $3s^23p^2\ ^3P$ - $3s^23p3d\ ^3D^o$ transition, but are larger than the measured value [19].

B. Wave functions for initial and final states of S^+

The S^+ initial $3s^23p^3\ ^4S^o$, $^2D^o$, and $^2P^o$ bound states and the final S^{2+} ion plus photoelectron states (^4P, ^2F, ^2D, ^2P, and ^2S) are represented by the same types of expansions. The nonorthogonal B-spline basis has been used to compute S^+ bound and continuum states. The initial states are described as bound states of the electron plus S^{2+} ion system. The wave function describing the S^+ $(N+1)$-electron system in an internal region surrounding the atom with radius r is expanded in terms of energy-independent functions [5,6]

$$\Psi_k = A\sum_{ij} a_{ijk}\overline{\Phi}_i u_j(r), \tag{1}$$

where $\overline{\Phi}_i$ are channel functions formed from the multiconfigurational functions of the S^{2+} target states and the operator A antisymmetrizes the wave function. The radial functions u_j are expanded in the B-spline basis as follows:

$$u_j(r) = \sum_i \overline{a_{ij}} B_i(r). \tag{2}$$

The coefficients a_{ijk} are now replaced by the coefficients $\overline{a_{ij}}$ which are determined by diagonalizing the $(N+1)$-electron Hamiltonian inside the R-matrix box. The final ^4P state is allowed by dipole selection rules in the photoionization of the ground $3s^23p^3\ ^4S^o$ state, while ^2P, ^2D, ^2F final states and ^2S, ^2P, ^2D final states are allowed in the photoionization process from the initial $3s^23p^3\ ^2D^o$ and $^2P^o$ states, respectively, in the LS-coupling scheme. In the intermediate coupling scheme, the $2J=1$, 3, 5, and 7 even parity final levels are allowed for the $2J=1$, 3, and 5 odd parity initial levels. The $(N+1)$-electron wave functions for the S^+ initial and final states are obtained by considering doublet and quartet symmetries for $L=0-4$ of both even and odd parities in the intermediate coupling. Additional spectroscopic and correlation orbitals have been obtained to improve the representation of the S^+ $3s^23p^3\ ^4S^o$, $^2D^o$, $^2P^o$ initial bound states and ^4P, ^2S, ^2P, ^2D, and ^2F final continuum states. Three separate sets of spectroscopic $3s$ and $3p$ orbitals and s, p, d, and f correlation orbitals have been determined to improve the correlation in the $3s^23p^3\ ^4S^o$, $^2D^o$, and $^2P^o$ bound states. Then separate set of s, p, d, and f correlation orbitals has been obtained for each S^+ final continuum state. The wave functions for the initial bound states and final continuum states are calculated using the one-electron orbitals used for the residual S^{2+} ionic states plus additional spectroscopic and correlation orbitals to improve the representation of initial and final states, with the addition of 91 B-spline continuum basis. The radius of the R-matrix box was chosen to be 46.5 a_0 to enclose the bound orbitals almost completely. The $(N+1)$-electron states have been described by all possible configurations generated by adding an electron to N-electron configurations plus the configurations generated with the additional orbitals that were obtained to improve initial and final states of S^+. Thus we attempted to account for the correlation effects adequately in a balanced way.

The initial state wave functions of S^+ are generated with closed-channel boundary conditions. The calculated ionization energies for the initial bound $3s^23p^3\ ^4S^o$, $^2D^o$, and $^2P^o$ states are 23.355, 21.533, and 20.293 eV, respectively, which are in excellent agreement with the measured values of 23.34, 21.50, and 20.30 eV. The calculated OP ionization energies are 23.627, 21.709, and 20.336 eV. The excellent

TABLE II. Oscillator strengths for dipole-allowed transitions among the S^{2+} states.

Transition	Present		Tayal[a]		Nahar[b]		
	f_L	f_V	f_L	f_V	f_L	f_V	Experiment
$3s^23p^2\ ^3P$-$3s3p^3\ ^3D^o$	0.024	0.021	0.023	0.020	0.024	0.021	0.022[c]
$3s^23p^2\ ^3P$-$3s3p^{33}P^o$	0.046	0.049	0.044	0.044	0.043	0.038	0.036[d]
$3s^23p^2\ ^3P$-$3s3p^3\ ^3S^o$	0.355	0.351	0.356	0.345	0.360	0.340	
$3s^23p^2\ ^1D$-$3s3p^3\ ^1D^o$	1.011	0.973	1.00	0.988	0.021	0.019	0.0167[c];0.99[e]
$3s^23p^2\ ^1D$-$3s3p^3\ ^1P^o$	0.338	0.337	0.357	0.371	0.38	0.37	
$3s^23p^2\ ^1S$-$3s3p^3\ ^1P^o$	0.007	0.006	0.001	0.0001	0.0023	0.0052	
$3s^23p^2\ ^3P$-$3s^23p3d\ ^3D^o$	1.667	1.627	1.658	1.615	1.670	1.630	0.96[f]
$3s^23p^2\ ^3P$-$3s^23p3d\ ^3P^o$	0.737	0.736	0.785	0.763	0.780	0.760	
$3s^23p^2\ ^1D$-$3s^23p3d\ ^1P^o$	0.011	0.013	0.020	0.016	0.024	0.024	
$3s^23p^2\ ^1D$-$3s^23p3d\ ^1D^o$	0.029	0.027	0.025	0.023	1.02	0.982	
$3s^23p^2\ ^1D$-$3s^23p3d\ ^1F^o$	1.364	1.322	1.33	1.31	1.36	1.35	
$3s^23p^2\ ^1S$-$3s^23p3d\ ^1P^o$	2.741	2.659	2.70	2.64	2.71	2.64	

[a]Reference [11].
[b]Reference [15].
[c]Reference [16].
[d]Reference [18].
[e]Reference [17].
[f]Reference [19].

agreement between our results and the experiment indicates the good quality of our initial state wave functions as well as the balanced account of correlation effects in the S^+ initial states and the S^{2+} ground state.

The oscillator strengths for transitions between the S^+ states can provide yet another test of the quality of wave functions. We have carried out a bound-bound *B*-spline *R*-matrix calculation to obtain oscillator strengths for dipole-allowed transitions in S^+ using the same basis functions as used in our photoionization calculation. We have listed these oscillator strengths in Table III where our results are compared with other reliable calculations [21–23]. Again a good agreement between length and velocity values as well as with other available calculated results can be noted, indicating that our wave functions are likely to be of good quality. The continuum cross sections away from resonances depend on the quality of one-electron radial functions. The lack of balance in correlation terms between the initial and final states can cause changes in the position and shape of resonances.

TABLE III. Oscillator strengths for dipole-allowed transitions among the S^+ states.

Transition	Present		Tayal[a]		RBS[b]		
	f_L	f_V	f_L	f_V	f_L	f_V	Ojha[c]
$3s^23p^3\ ^4S^o$-$3s3p^4\ ^4P$	0.032	0.028	0.031	0.030	0.038	0.038	0.033
$3s^23p^3\ ^4S^o$-$3s^23p^24s\ ^4P$	0.398	0.398	0.396	0.369	0.379	0.367	0.420
$3s^23p^3\ ^4S^o$-$3s^23p^23d\ ^4P$	2.293	2.248	2.259	2.118	2.249	2.150	2.262
$3s^23p^3\ ^4S^o$-$3s^23p^25s\ ^4P$	0.053	0.053					
$3s^23p^3\ ^4S^o$-$3s^23p^24d\ ^4P$	0.535	0.526					
$3s^23p^3\ ^4S^o$-$3s^23p^26s\ ^4P$	0.017	0.017					
$3s^23p^3\ ^4S^o$-$3s^23p^25d\ ^4P$	0.172	0.170					
$3s^23p^3\ ^4S^o$-$3s^23p^27s\ ^4P$	0.008	0.008					
$3s^23p^3\ ^4S^o$-$3s^23p^26d\ ^4P$	0.075	0.074					
$3s^23p^3\ ^4S^o$-$3s^23p^28s\ ^4P$	0.005	0.005					
$3s^23p^3\ ^4S^o$-$3s^23p^27d\ ^4P$	0.048	0.047					
$3s^23p^3\ ^4S^o$-$3s^23p^27s\ ^4P$	0.007	0.007					
$3s^23p^3\ ^4S^o$-$3s^23p^26d\ ^4P$	0.045	0.045					

[a]Reference [23].
[b]Reference [22].
[c]Reference [21].

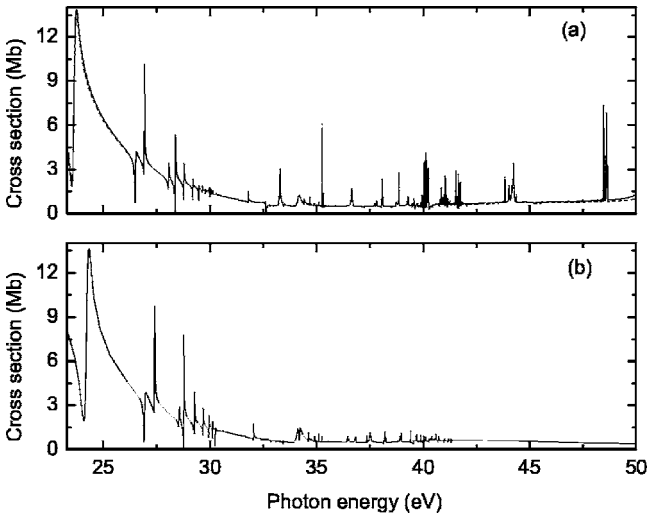

FIG. 1. Photoionization cross section from ground $^4S^o$ state as a function of photon energy from the S^{2+} ^3P threshold at 23.3 to 50 eV. (a) Solid curve, present length values from 27-state *LS* calculation; dashed curve, present velocity values from 27-state *LS* calculation; (b) OP calculation.

C. Resonance parameters

The effective quantum number n^* is expressed relative to the assigned thresholds as follows:

$$n^* = \frac{(Z-N)}{(E_t - E_r)^{(1/2)}}, \tag{3}$$

where Z is the atomic number, N is the number of electrons in the ion, E_t is the threshold energy, and E_r is the corresponding resonance energy. The diagonalization of the K matrix in the space of open channels N_o gives eigenvalues λ_i that are used to define eigenphase in each channel as follows:

$$\delta_i = \tan^{-1}\lambda_i, \quad i = 1,2,\ldots,N_o. \tag{4}$$

The eigenphase sum δ is obtained by adding δ_i for all open channels. A resonance position E_r is defined as the energy at which the eigenphase sum δ has a maximum value of $\frac{d\delta}{dE}$ and resonance widths are related to the inverse of the eigenphase gradients as discussed by Quigley and Berrington (QB) [24] in the QB method of resonance analysis using the R-matrix method.

III. RESULTS AND DISCUSSION

A. Photoionization cross sections

Photoionization cross sections from the S^+ ground $3s^23p^3$ $^4S^o$ and metastable $^2D^o$ and $^2P^o$ states for leaving the S^{2+} ion in the lowest 27 *LS* terms are calculated in both length and velocity formulations of the dipole matrix elements in the region of autoionizing resonances in the nonrelativistic B-spline R-matrix approach [5,6]. We have compared length and velocity cross sections for photoionization from the ground state as a function of photon energy in Fig. 1(a). The length and velocity results are shown by solid and dashed curves, respectively. There is normally an excellent agreement between the length and velocity results and the two curves are almost superimposed. The agreement between the length and velocity results for most photon energies is well within 5%. This agreement provides some indication that our cross sections are likely to be accurate. The cross section shows significant structure with a broad maximum just above the first ionization threshold. The background cross section away from resonances shows a decreasing trend from threshold to about 36.3 eV and a very gradual increasing trend after that. There are several prominent Rydberg series of resonances culminating at various S^{2+} thresholds of quintet and triplet symmetries. The $3s3p^3(^5S^o, ^3D^o, ^3P^o, ^3S^o)np$ ^4P, $3s^23p3d(^3F^o)nf$ ^4P, $3s^23p3d(^3P^o, ^3D^o)np$ ^4P, and $3s^23p4s(^3P^o)np$ ^4P Rydberg series produce dominant resonance features in the energy region from threshold to 42 eV. Photoionization leading to the S^{2+} $3s3p^3$ $^5S^o$, $^3D^o$, $^3P^o$, and $^3S^o$ thresholds is due to single-electron $3s \rightarrow np$ and $3s \rightarrow nf$ transitions. Photoionization leading to the S^{2+} higher excited states is mostly due to two-electron transitions that require photoionization plus excitation. The two-electron transition process is less likely than the single-electron transition process and, therefore, relatively weaker resonances in the higher energy region than in the lower energy region.

The calculated cross sections for photoionization of S^+ in the ground $3s^23p^3$ $^4S^o$ state from the opacity project (OP) are shown in Fig. 1(b). The states belonging to the S^{2+} $3s^23p^2$, $3s3p^3$, and $3s^23p3d$ configurations were included in the OP calculations. There is a very good agreement between the two calculations for continuum cross sections. However, there are significant discrepancies in resonance structures. There are deviations in the position, width, and peak value of resonances. Additional resonances in our calculation can be seen as we performed our calculation at a fine-energy mesh to resolve resonances and included additional resonance features converging on higher S^{2+} thresholds. The deviation between the two calculations is caused by the differences in wave functions to represent S^+ initial bound and final continuum states and S^{2+} residual ionic thresholds.

We have also performed a 17-state nonrelativistic B-spline R-matrix calculation. The 27-state and 17-state calculations agree remarkably well except for additional weak resonance structures converging to the $3s^23p4d$ thresholds in the 27-state calculation. We have carried out a semirelativistic Breit-Pauli calculation which includes 31 fine-structure levels of the 17 *LS* terms. Relativistic effects such as the one-body mass correction, the Darwin term, and spin-orbit interaction are included through the Breit-Pauli Hamiltonian in intermediate coupling. Inclusion of spin-orbit interaction in the Breit-Pauli approximation introduces more autoioinizing series of resonances culminating at the increased number of S^{2+} thresholds than the nonrelativistic *LS* calculation. In a recent merged ion-photon beam experiment with the synchrotron-radiation from an undulator measured major autoionizing resonance features [3], the detailed Breit-Pauli results for photoioinzation from the ground $3s^23p^3$ $^4S^o_{3/2}$ level are compared with the measured cross sections in Fig. 2 to display the Rydberg series of resonances converging on various S^{2+} thresholds between 23.3 and 42 eV. The upper panel shows the theoretical results and the lower panel shows mea-

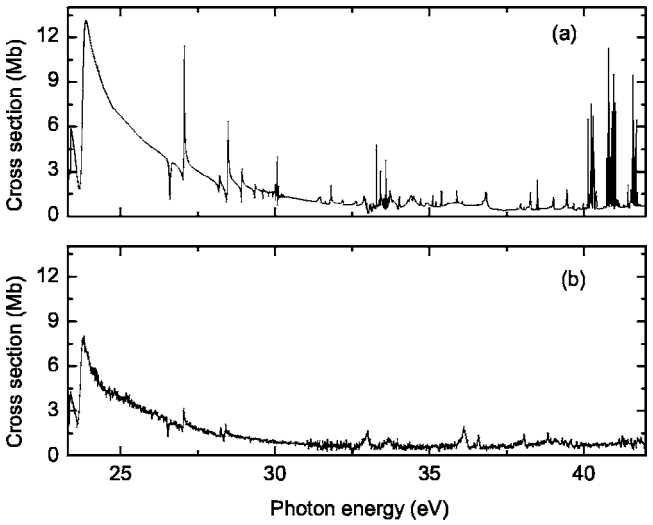

FIG. 2. Photoionization cross section from ground $^4S^o$ state as a function of photon energy from the S^{2+} ^3P threshold at 23.3 to 42 eV. (a) Present length values from 31-level Breit-Pauli calculation; (b) measured cross section [3].

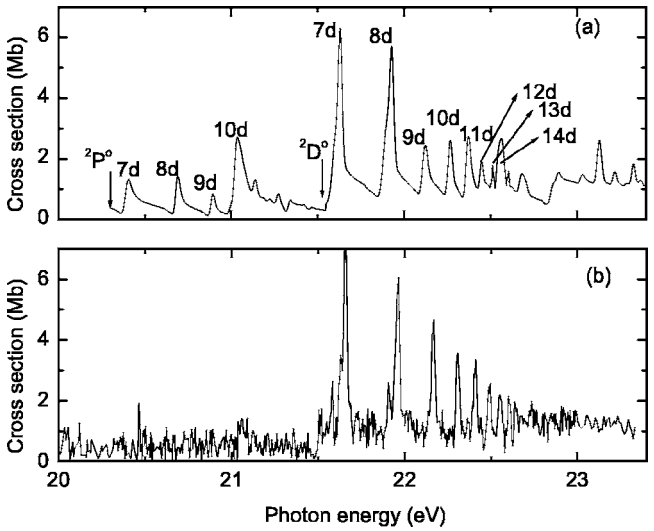

FIG. 3. Cross sections below the S^{2+} ^3P threshold at 23.3 eV due to photoionization from the S^+ $^2D^o$ and $^2P^o$ metastable states. (a) Weighted sum of our convoluted photoionization cross section from Breit-Pauli calculation; (b) measured cross section [3].

sured values. The $3s3p^3(^5S^o)np$ ^4P Rydberg series culminates on the $3s3p^3$ $^5S^o$ threshold and $3s3p^3(^3P^o)np$ ^4P and $3s3p^3(^3S^o)np$ ^4P Rydberg series culminate on the $3s3p^3$ $^3P^o$ and $3s3p^3$ $^3S^o$ thresholds, respectively. The $3s3p^3(^3D^o)np,nf$ ^4P Rydberg series converge on the $3s3p^3$ $^3D^o$ threshold and $3s^23p3d(^3F^o)nf$ ^4P Rydberg series converge on the $3s^23p3d$ $^3F^o$ threshold. In addition, lower members of the $3s^23p4s(^3P^o)np$, $3s^23p3d(^3P^o)np$, and $3s^23p3d(^3D^o)np,nf$ Rydberg series lie in the energy region below the $3s3p^3$ $^3S^o$ threshold. Owing to several interacting Rydberg resonance series converging on different S^{2+} thresholds, the resonance structures are quite complex. The photoionization cross sections have been calculated at a very fine energy grid of 2.2×10^{-5} eV to resolve resonances including narrow sharp resonances.

In order to make a meaningful comparison with the experiment, we convoluted the calculated resonances with a Gaussian distribution function of the monochromometer bandwidth of the experiment in the photoionization from the S^+ $3s^23p^3$ $^4S^o$, $^2D^o$, $^2P^o$ initial bound states and then obtained a weighted sum of convoluted cross sections using the beam composition of the experiment. The ion beam contained an admixture of the $^4S^o$, $^2D^o$, and $^2P^o$ states with a composition of 81% S^+ ions in the $^4S^o$ state, 15% S^+ ions in the $^2D^o$state and 4% S^+ ions in the $^2P^o$ state. The measured line shape and peak cross section of the resonance features depend on the instrumental bandpass and spectrometer slit function. The weighted sum of convoluted cross sections is compared in Figs. 3–5 with the measured cross sections of Kristensen *et al.* [3]. Since the present results in both length and velocity formulations of the dipole matrix elements agree very well with each other, we have used length results to compare with the experiment. We used a function of constant full width at half maximum of 25 meV below 23.3 eV and a constant 35 meV above this energy. It should be emphasized that the resolution of the experiment does not remain constant and varies with photon energy. We have displayed a weighted sum of the convoluted photoionization cross sections as a function of photon energy in Fig. 3 in the photon energy region from 20.3 to 23.3 eV together with the measured values. The cross sections in this energy region are entirely due to the photoionization from the S^+ metastable $^2D^o$ and $^2P^o$ states. The calculated S^+ $3s^23p^{22}P^o$ and $^2D^o$ ionization thresholds occur at 20.29 and 21.53 eV and are shown by down arrows in the upper panel of Fig. 3. The cross sections below the ionization threshold at 21.53 eV are due to photoionization from the $3s^23p^3$ $^2P^o$ metastable state and the resonance structure is due to $3s^23p^2(^1D)nd$ ^2P and ^2D Rydberg

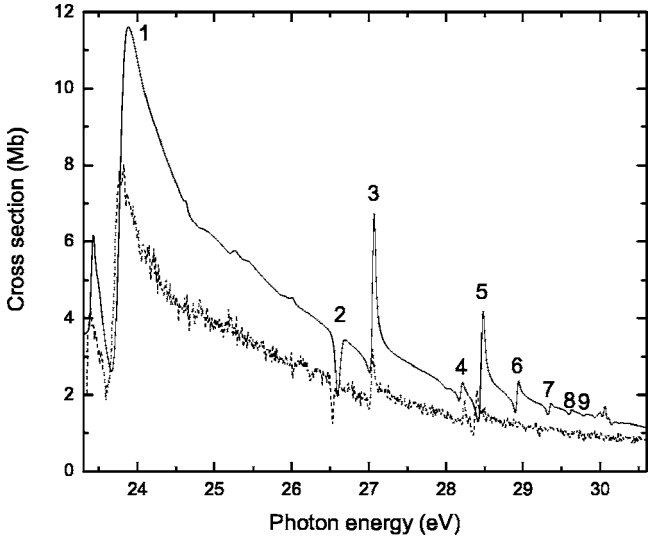

FIG. 4. Cross sections between the S^{2+} ^3P threshold at 23.3 eV and $3s3p^3$ $^5S^o$ threshold at 30.6 eV for photoionization from the S^+ $^4S^o$ ground state. Solid curve, weighted sum of our convoluted photoionization cross section from the Breit-Pauli calculation; dashed curve, measured cross section [3].

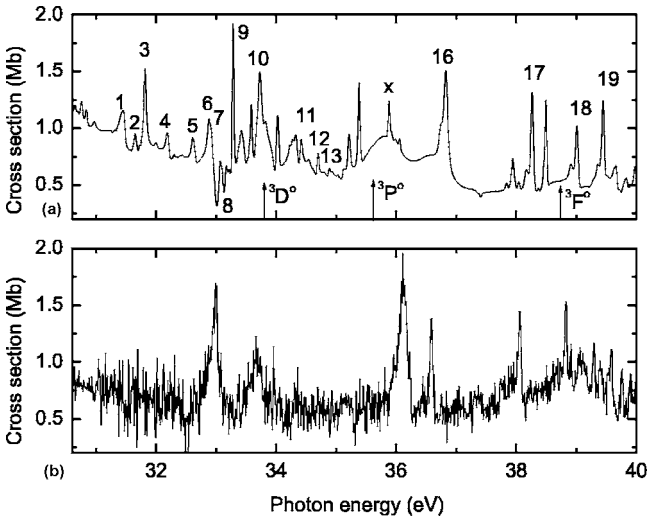

FIG. 5. Cross sections between the S^{2+} $^5S^o$ threshold at 30.6 eV and $^3S^o$ threshold at 40.6 eV for photoionization from the S^+ $^4S^o$ ground state. (a) Weighted sum of our convoluted photoionization cross section from the Breit-Pauli calculation; (b) measured cross section [3].

series. The $3s^23p^2(^1D)nd$ ^2P, ^2D,^2F and $3s^23p^2(^1D)ns^2D$ Rydberg series occur above 21.53 eV in the photoionization from the $3s^23p^3$ $^2D^o$ metastable state. The calculated resonance structures show reasonable agreement with experiment. The $3s^23p^2(^1D)nd$ Rydberg series are the dominant resonance features in this photon energy region. The higher members of the $3s^23p^2(^1D)nd$ Rydberg series overlap with each other. The convoluted peak of many $3s^23p^2(^1D)nd$ resonances in our calculation is smaller than the experiment. A part of the discrepancy may have been caused by the use of the constant Gaussian distribution function (25 meV) to convolute the resonances.

The continuum cross sections from the S^+ metastable $3s^23p^3$ $^2D^o$ and $^2P^o$ states leading to the S^{2+} states compare very well with OP calculations in the photon energy region from threshold to 23.3 eV (not shown). However, there are significant discrepancies in the position of resonances between the two calculations caused again by differences in wave functions that lead to inaccurate thresholds in the OP calculation. The OP calculation resolved only the lower members of the various Rydberg series.

The weighted sum of convoluted cross sections between the $3s^23p^2$ ^3P threshold at 23.3 eV and $3s3p^3$ $^5S^o$ threshold at 30.5 eV is compared with measured results in Fig. 4. The $3s3p^3(^5S^o)np$ ^4P Rydberg series culminates on the $3s3p^3$ $^5S^o$ threshold in this energy region. The lowest two members of the $3s3p^3(^3D^o)np$ ^4P resonance series leading to the $3s3p^3$ $^3D^o$ threshold, and the lowest member of the $3s3p^3(^3P^o)np$ ^4P Rydberg series leading to the $3s3p^3$ $^3P^o$ threshold also appear below the $3s3p^3$ $^5S^o$ threshold. The interactions of the $3s3p^3(^5S^o)np$ and $3s3p^3(^3P^o)3p$ Rydberg states with continuum produce upward jump in cross sections and the interaction of the $3s3p^3(^3D^o)3p$ Rydberg state with continuum produces a downward jump in cross sections. As a result the $3s3p^3(^3D^o)3p$ ^4P resonance state appears as a window resonance. The $3s3p^3(^3P^o)3p$ and $3s3p^3(^3D^o)3p$,$4p$ resonance states produce a strong perturbation in the $3s3p^3(^5S^o)np$ series. The small bumps in our weighted cross sections in the low energy region are due to resonance states which occur in the photoionization from the metastable $^2D^o$ and $^2P^o$ states. There are substantial discrepancies between theory and experiment for the continuum cross sections; the calculated results are larger than the experiment. Theoretical positions of resonance states are in reasonable agreement with experiment but there are significant discrepancies in the peak and width of the resonances. The peak value of the calculated cross section for the broad resonance feature just above the threshold is about 45% larger than the measured value. We have performed several test calculations to check the sensitivity of the width and peak of the resonance state to correlation in the initial and final states, and found approximately the same results. The cause of discrepancy is not clear. The radiation damping can affect the peak and width of resonances, particularly for the high-n resonances [25,26]. The radiation damping is found to have insignificant influence on the resonance structures in our calculation. The OP results are also larger than the experiment in this energy region. There is a good agreement between the two calculations except for a shift in the position of resonances due to the differences in thresholds and wave functions in the two calculations.

The weighted sum of convoluted cross sections in the photon energy range between the $3s3p^3$ $^5S^o$ and $3s3p^3$ $^3S^o$ thresholds is displayed in Fig. 5. It is evident that the Rydberg series leading to the S^{2+} $3s3p^3$ $^3D^o$, $3s^23p3d$ $^3F^o$, and $3s3p^3$ $^3S^o$ thresholds do not exhibit regular patterns. This is due to perturbations caused by overlapping $3s3p^3(^3D^o)np$,nf, and $3s3p^3(^3P^o)np$ resonance series leading up to the S^{2+} $3s3p^3$ $^3D^o$ and $^3P^o$ excitation thresholds and by the interacting $3s^23p3d(^3F^o)nf$ and $3s3p^3(^3S^o)np$ series culminating on $^3F^o$ and $^3S^o$ thresholds. The $^3D^o$, $^3P^o$, and $^3F^o$ thresholds are indicated by arrows in Fig. 5. The $3s3p^3(^3P^o)np$ $(n=4-6)$ resonance states of the series culminating on $^3P^o$ threshold appear below the $3s3p^3$ $^3D^o$ threshold and strongly interact with the $3s3p^3(^3D^o)np$ Rydberg series and produce significant irregularities. The $3s3p^3(^3P^o)6p$ resonance state lies close to the $^3D^o$ threshold and interacts with the higher members of the $3s3p^3(^3D^o)np$,nf Rydberg series as well as with the next member of the series which lie above the $^3D^o$ threshold. The $3s3p^3(^3P^o)np$ series between the $^3D^o$ and $^3P^o$ thresholds displays approximately a regular pattern. Higher members of the series which lie close to the $^3P^o$ threshold lump together to give a large feature below the threshold in the convoluted cross sections. The $3s^23p3d(^3F^o)nf^4P$ resonance states occur between the $3s3p^3$ $^3P^o$ and $3s^23p3d$ $^3F^o$ thresholds. The lower members of several $3s^23p4s(^3P^o)np$, $3s^23p3d(^3P^o)np$, and $3s^23p3d(^3D^o)np$,nf Rydberg series culminating at closely spaced S^{2+} excitation thresholds can also be seen in this energy region. These members interfere with higher members $(n \geq 14)$ of the $3s3p^3(^3S^o)np$ Rydberg series and produce irregularities in the series.

Several qualitative and quantitative differences between the measured and calculated resonances can be seen in Fig.

5. It may be noted that we used a constant Gaussian distribution function of 35 meV in this energy region to convolute the resonances, while the resolution of the experiment gradually increases with increasing energy. The resonance structure in the experiment appears to be more complex than the theory because of the noise in measured cross sections. There are significant discrepancies in the positions and widths of resonances in this energy region. On the theoretical side, discrepancies may be caused by the lack of convergence or completeness of the expansions used for the description of N- and $(N+1)$-electron atomic systems in our calculation. The imbalance between these expansions may influence the calculated positions and line shapes of resonances. The wave functions perhaps are not sufficiently flexible to accurately represent interactions between Rydberg series and perturber states and relaxation effects. On the experimental part, instrumental bandpass and spectrometer slit function may introduce uncertainties in the measured line shape and peak cross sections. There may also be uncertainties in the beam composition. The calculated continuum cross sections are larger than the experiment in the photon energy region up to about 37.0 eV and lower thereafter. The measured cross section shows a decreasing trend up to 33.7 eV where a minimum in cross section is observed. Kristensen *et al.* [3] characterized the minimum as a Cooper minimum. However, this minimum does not appear to represent a true dip in a continuum cross section to constitute a Cooper minimum. Our calculated cross sections display a gradual decreasing trend with a minimum in cross section around 36.5 eV which is shifted to a higher energy side by 2.8 eV with respect to experimental value. The OP calculations underestimate the continuum cross section in this photon energy region. The OP cross section does not include any closed channels in the energy region above 40.5 eV in the limited basis set calculations. There is an unidentified large resonance feature in the experiment at 36.13 eV and our calculation shows the $3s^23p3d(^3F^o)4f\ ^4P$ resonance state at 35.89 eV (marked X in Fig. 5) in its neighborhood just above the $^3P^o$ threshold. Our calculation suggests that the unidentified feature in the experiment may be due to the $3s^23p3d(^3F^o)4f\ ^4P$ resonance state. The calculated position of this resonance state is shifted by about 0.2 eV because of the inaccuracy in the theoretical $3s^23p3d\ ^3F^o$ threshold.

B. Resonance analysis

The resonances are scanned at a very fine energy mesh based on quantum defect. We have analyzed lower members of the $3s^23p^2(^1D)ns,nd$ autoionizing resonance series culminating at the $S^{2+}\ 3s^23p^2\ ^1D$ threshold in the photoioinization from the metastable $^2D^o$ and $^2P^o$ states. The positions E_r, widths Γ_r, and effective quantum numbers n^* are listed in Table IV and compared with the experimental values of Kristensen *et al.* [3]. Below 21.53 eV there are two major $3s^23p^2(^1D)nd\ ^2P$ and ^2D resonance series and their members occur at the same position. We have identified lower members of the $nd\ ^2P^o$ and $^2D^o$ $(n=7-10)$ series in Fig. 3. The $3s^23p^2(^1D)ns\ ^2D$ and $3s^23p^2(^1D)nd\ ^2P$, ^2D, and ^2F resonance series can be easily identified above 21.53 eV. The

TABLE IV. Resonance parameters of $3s^23p^2(^1D)ns$, nd, nf series.

		Present			Experiment
Index	State	E_r (eV)	Γ_r (meV)	n^*	E_r (eV)
1	7d ^2P, ^2D	20.40			
2	8d ^2P, ^2D	20.69			
3	9d ^2P, ^2D	20.89			
4	10d ^2P, ^2D	21.04			
5	7s ^2D	21.54	0.07	6.440	21.58
6	7d ^2F	21.59	46.1	6.562	21.63
7	7d ^2P	21.63	25.6	6.681	21.66
8	7d ^2D	21.64	3.9	6.689	21.73
9	8s ^2D	21.87	0.05	7.442	21.91
10	8d ^2F	21.90	28.2	7.561	21.96
11	8d ^2P	21.93	15.9	7.679	21.96
12	8d ^2D	21.93	2.6	7.682	
13	9s ^2D	22.09	0.04	8.443	
14	9d ^2F	22.11	18.6	8.561	22.17
15	9d ^2P	22.13	10.6	8.677	22.17
16	9d ^2D	22.13	1.9	8.678	22.17
17	10s ^2D	22.24	0.04	9.444	
18	10d ^2F	22.26	12.9	9.560	22.31
19	10d ^2P	22.27	7.4	9.675	22.31
20	10d ^2D	22.27	0.8	9.680	22.31
21	11s ^2D	22.35	0.01	10.445	
22	11d ^2F	22.36	9.3	10.559	22.41
23	11d ^2P	22.37	5.4	10.674	22.41
24	11d ^2D	22.37	0.7	10.672	22.41
25	12d ^2F	22.44	7.0	11.559	22.49
26	12d ^2P	22.45	4.1	11.673	22.49
27	12d ^2D	22.45	0.6	11.670	22.49
28	13d ^2F	22.51	5.3	12.559	22.55
29	13d ^2P	22.51	3.1	12.673	22.55
30	13d ^2D	22.51	0.5	12.669	22.55
31	14d ^2F	22.55	4.2	13.558	22.61
32	14d ^2P	22.56	2.5	13.672	22.61
33	14d ^2D	22.56	0.4	13.668	22.61
34	15d ^2F	22.60	3.4	14.558	22.65
35	15d ^2P	22.60	2.0	14.673	22.65
36	15d ^2D	22.60	0.3	14.668	22.65

$3s^23p^2(^1D)ns\ ^2D$ series is very weak and we have identified its lower members. Among the three $3s^23p^2(^1D)nd$ Rydberg resonance series, the ^2F series is the strongest followed by the ^2P and ^2D series. Higher members of the $nd\ ^2F$, ^2P, and ^2D series almost coincide in position. The $nd\ ^2F$ Rydberg series encompasses the $nd\ ^2P$ and ^2D series. The calculated positions of resonances are on average 0.05 eV lower than the measured values. The difference is caused by a slightly under correlated initial $3s^23p^3\ ^2D^o$ bound state compared to the final continuum states. The Rydberg resonance series exhibit regular patterns with a nearly constant value of quan-

TABLE V. Resonance parameters of $3s3p^3(^5S^o, {}^3D^o, {}^3P^o)np$ series.

		Present			Experiment			OP	
Index	State	E_r (eV)	Γ_r (meV)	n^*	E_r (eV)	Γ_r (meV)	n^*	E_r (eV)	Γ_r (meV)
1	$3s3p^3(^5S^o)3p$	23.78	220	2.843	23.70	150	2.806	24.22	240
2	$3s3p^3(^3D^o)3p$	26.59	44	2.740	26.52	18	2.742	26.94	47
3	$3s3p^3(^5S^o)4p$	27.05	24	3.965	27.04	23	3.903	27.41	24
4	$3s3p^3(^3P^o)3p$	28.20	16	2.707	28.23	9	2.721	28.56	18
5	$3s3p^3(^5S^o)5p$	28.48	13	5.175	28.38	29	4.938	28.78	13
6	$3s3p^3(^5S^o)6p$	28.93	13	5.864					
7	$3s3p^3(^5S^o)7p$	29.34	7.6	6.813					
8	$3s3p^3(^5S^o)8p$	29.61	4.9	7.765					
9	$3s3p^3(^5S^o)9p$	29.79	3.4	8.679					
10	$3s3p^3(^5S^o)10p$	29.93	2.6	9.666					
11	$3s3p^3(^3D^o)4p$	30.02	1.4	3.780					

tum defects. The quantum defect for the $3s^23p^2(^1D)ns$ Rydberg series is around 0.56, while for the $3s^23p^2(^1D)nd\,^2F$, ^2P, and ^2D Rydberg series the quantum defects are around 0.44, 0.325, and 0.320, respectively.

Our calculated positions, widths, and effective quantum numbers for resonance states between the $3s^23p^2\ ^3P$ and $3s3p^3\ ^5S^o$ thresholds are listed in Table V together with the measured values and the results from the OP calculation. The $3s3p^3(^5S^o)np\ ^4P$ resonance series culminates on the $3s3p^3\ ^5S^o$ threshold and there are three interlopers in this energy region. Two of the interlopers belong to the $3s3p^3(^3D^o)np$ series and the third interloper is the lowest member of the $3s3p^3(^3P^o)np$ series converging on the $3s3p^3\ ^3P^o$ threshold. We have labeled the resonance states in the figure according to the indices in Table V. In our calculation resonances 2, 4, and 11 are identified as interlopers. The presence of the $3s3p^3(^3D^o)3p$ and $3s3p^3(^3P^o)3p$ interlopers perturbs the $3s3p^3(^5S^o)4p$, 5p resonance states substantially as indicated by the deviations in quantum defects for these states. The quantum defects for the unperturbed members of the series appear to be around 0.2, while for the perturbed $3s3p^3(^5S^o)4p$ state the quantum defect is 0.035. The effective quantum numbers for the resonance states from the experiment are also listed in Table V. There is a reasonable agreement between the present theory and experiment except for the $3s3p^3(^5S^o)5p$ resonance state which appears to be pushed to higher energy by the interaction with the interloper $3s3p^3(^3P^o)3p$ in our calculation. The calculated quantum defect ($\sim$0.20) for the $3s3p^3(^5S^o)np$ Rydberg states compare well with the experiment ($\sim$0.23) [3]. The interloper $3s3p^3(^3D^o)4p$ is positioned at 30.02 eV in our calculation and it greatly perturbs the higher members of the $3s3p^3(^5S^o)np$ ($n\geq 9$) Rydberg series. The quantum defect of the higher members again shows significant variation from the 0.2 value. The $3s3p^3(^3D^o)3p$ resonance state appears as a window resonance due to repulsive interaction between the Rydberg state and continuum [7,8] and can be clearly seen in Fig. 4 (upper panel). The $3s3p^3(^5S^o)3p$, $3s3p^3(^3D^o)3p$, and $3s3p^3(^3P^o)3p$ resonance states correspond to intrashell transitions and, therefore, have larger widths than other resonances in Table V. The calculated position of broad resonance feature close to the $3s^23p^2\ ^3P$ threshold is slightly higher (0.08 eV) than the experiment. However, there are substantial discrepancies in the width and peak of the resonance state. The calculated width is 53% larger than the experiment. Our results agree with OP calculation for the width and peak value.

We identify the second resonance feature as $3s3p^3(^3D^o)3p\ ^4P$ state. The calculated position and shape of this feature agree with the experiment, but the calculated width is larger. The larger width indicates a stronger interaction between the Rydberg state and the continuum. The third feature is identified as $3s3p^3(^5S^o)4p$ resonance state which appears between the $3s3p^3(^3D^o)3p$ and $3s3p^3(^3P^o)3p$ interlopers, and is strongly perturbed. The calculated position is higher than the experiment by 0.07 eV. The width is in excellent agreement with the experiment. The position of the fourth feature (an interloper) agree very well with the measured value. The position of the fifth resonance feature $3s3p^3(^5S^o)5p$ is higher by 0.1 eV than the experiment and it is narrower in our calculation. The position of these resonances in the OP calculation is shifted to a higher side by about 0.4 eV compared to our calculation and experiment. The widths in two calculations agree well. It may also be noted that the relative separation between the resonance states in the present work and OP calculation as well as in the experiment compare very well. The separations between 1 and 2, 2 and 3, 3 and, 4 and between 4 and 5 resonance states are 2.81, 0.46, 1.15, and 0.28 eV in our calculation; 2.82, 0.52, 1.19, and 0.15 in the experiment and 2.72, 0.47, 1.15, and 0.22 eV in the OP calculation. The larger separation between resonance states 4 and 5 in our work may have been caused by a slightly over correlated final continuum state.

The shape and correlation parameters and oscillator strengths of the lower five resonance lines are listed in Table VI where our results are compared with the measured results [3] and OP calculation. The shape parameter q is negative for the $3s3p^3(^3D^o)3p\ ^4P$ window resonance and positive for other four resonance lines. The sign of q in our calculation for the window feature agrees with the experiment but differs with the OP calculation. Our results for the q and ρ^2 are in

TABLE VI. Resonance shape and correlation parameters.

		Present			Experiment			OP		
Index	State	q	ρ^2	$f\times10^{-3}$	q	ρ^2	$f\times10^{-3}$	q	ρ^2	$f\times10^{-3}$
1	$3s3p^3(^5S^o)3p$	0.99	0.54	31	1.0	0.63	9.0	1.0	0.77	27
2	$3s3p^3(^3D^o)3p$	-0.36	0.40	0.07	-0.24	0.73	0.04	0.43	0.86	0.47
3	$3s3p^3(^5S^o)4p$	2.74	0.18	1.5	1.9	0.20	0.68	3.1	0.22	2.7
4	$3s3p^3(^3P^o)3p$	1.16	0.26	0.41	2.5	0.16	0.25	1.6	0.26	0.46
5	$3s3p^3(^5S^o)5p$	1.48	0.50	0.61	1.2	0.35	0.39	1.9	0.98	0.15

good agreement with the experiment for the $3s3p^3(^5S^o)5p$ resonance line but the f value from our calculation is substantially larger. There is a reasonable agreement for the ρ^2 parameter for the $3s3p^3(^5S^o)4p$, $5p$, and $3s3p^3(^3P^o)3p$ resonance lines between theory and experiment but differences for the q parameters and f values exist.

The resonance parameters for the $3s3p^3(^3D^o)np,nf$, $3s3p^3(^3P^o)np$, and $3s3p^3(^3S^o)np$ Rydberg series are listed in Table VII and these are identified in Fig. 5 with the indices of Table VII as labels. The $3s3p^3(^3D^o)np,nf$ series culminates on S^{2+} $^3D^o$ threshold. The $3s3p^3(^3D^o)np$ Rydberg series is much stronger than the $3s3p^3(^3D^o)nf$ series and we have listed only the lowest member of the latter in Table VII. In addition there are three $3s3p^3(^3P^o)np$ $(n=4-6)$ interlopers in the energy region below the $^3D^o$ threshold. All three interlopers belong to the Rydberg series that culminates on the $^3P^o$ threshold and they produce significant perturbation in the $3s3p^3(^3D^o)np$ series. The $3s3p^3(^3P^o)5p$ interloper in particular produces irregularities in the shape and width of nearby resonance states. The $3s3p^3(^3P^o)5p$ resonance state lies very close to the $3s3p^3(^3D^o)8p$ state. The $3s3p^3(^3P^o)6p$ resonance state is identified below the $^3D^o$ threshold at 33.8 eV and it possibly has a wing above the threshold. The higher members of the $3s3p^3(^3P^o)np$ $(n\geq7)$ series appear in between the $^3D^o$ and $^3P^o$ thresholds and exhibit approximately a regular behavior. The higher members of the $3s3p^3(^3D^o)np$ and $3s3p^3(^3P^o)np$ series culminating on their respective thresholds lump together in the convoluted cross sections and give rise to large features below thresholds.

The $3s3p^3(^3S^o)np$ Rydberg series is also strong and its lowest two members occur below the $3s^23p3d$ $^3F^o$ threshold. The discrepancies in the position of $3s3p^3(^3S^o)np$ resonances with experiment are caused by the inaccuracy in the calculated excitation threshold of the S^{2+} $3s3p^3$ $^3S^o$ state. The calculated $^3S^o$ threshold is approximately 0.2 eV above the measured value. The calculated quantum defect for the $3s3p^3(^3S^o)np$ Rydberg series is approximately 0.29 which agrees well with the measured quantum defect of 0.26 [3].

TABLE VII. Resonance parameters of $3s3p^3(^3D^o,\ ^3P^o)np,nf$ series.

		Present			Experiment
Index	State	E_r (eV)	Γ_r (meV)	n^*	E_r (eV)
1	$3s3p^3(^3D^o)5p$	31.43	26.4	4.755	
2	$3s3p^3(^3D^o)5f$	31.64	0.3	4.994	
3	$3s3p^3(^3P^o)4p$	31.80	14.8	3.765	
4	$3s3p^3(^3D^o)6p$	32.15	12.2	5.722	
5	$3s3p^3(^3D^o)7p$	32.59	7.2	6.645	
6	$3s3p^3(^3P^o)5p$	32.88	4.6	4.450	33.00
7	$3s3p^3(^3D^o)8p$	32.91	5.2	7.662	
8	$3s3p^3(^3D^o)9p$	33.13	3.2	8.774	
9	$3s3p^3(^3D^o)10p$	33.27	2.6	9.797	
10	$3s3p^3(^3P^o)6p$	33.72	7.8	5.340	33.67
11	$3s3p^3(^3P^o)7p$	34.42	8.7	6.751	
12	$3s3p^3(^3P^o)8p$	34.69	6.4	7.674	
13	$3s3p^3(^3P^o)9p$	34.88	5.2	8.610	
14	$3s3p^3(^3P^o)10p$	35.02	4.1	9.570	
15	$3s3p^3(^3P^o)11p$	35.11	1.9	10.389	
16	$3s3p^3(^3S^o)4p$	36.80	52.0	3.752	36.58
17	$3s3p^3(^3S^o)5p$	38.24	27.8	4.736	38.05
18	$3s3p^3(^3S^o)6p$	38.99	26.1	5.698	38.83
19	$3s3p^3(^3S^o)7p$	39.43	23.4	6.636	

Lower members of the $3s^2 3p 4s(^3P^o)np$ and $3s^2 3p 3d(^3P^o, ^3D^o)np$ resonance series appear below the $3s3p^3\ ^3S^o$ threshold. However, these resonance states are weak.

IV. SUMMARY

We have presented fairly extensive nonrelativistic and Breit-Pauli *B*-spline *R*-matrix calculations for photoionization from the ground $3s^2 3p^3\ ^4S^o$ and excited metastable $^2D^o$ and $^2P^o$ states of S^+. The resonance series below the first ionization threshold at 23.3 eV exhibit almost regular patterns, while resonance structures culminating on $3s3p^3\ ^5S^o$, $^3D^o$, and $^3S^o$ thresholds show irregular patterns owing to strong interactions between the resonance series converging to thresholds and interlopers. A good overall agreement with OP calculations for continuum cross section is noted. However, significant quantitative differences in resonance structures are seen with OP results. The lower members of the $3s^2 3p^2(^1D)ns, nd$ and $3s3p^3(^5S^o, ^3D^o, ^3P^o, ^3S^o)np$ resonance series are identified and their positions, widths and effective quantum numbers are listed. The calculated resonance structures show some qualitative and quantitative differences with the recent experiment [3]. There are significant differences in positions, widths and peak values of some of the resonances between theory and experiment. Substantial discrepancies for the continuum cross sections have been noted. Further experimental and theoretical works are needed to resolve these discrepancies. Our results should be useful in astrophysical applications.

ACKNOWLEDGMENTS

This research work is supported by NASA Grant No. NNG06GD39G from the Astronomy and Physics Research Analysis program.

[1] M. A. McGrath, P. D. Feldman, D. F. Strobel, H. W. Moos, and G. E. Ballester, Astrophys. J. **415**, L55 (1993).
[2] G. A. Doschek and U. Feldman, Astrophys. J. **315**, L67 (1987).
[3] B. Kristensen, T. Andersen, F. Folkmann, H. Kjeldsen, and J. B. West, Phys. Rev. A **65**, 022707 (2002).
[4] K. A. Berrington, W. B. Eissner, and P. H. Norrington, Comput. Phys. Commun. **92**, 290 (1995).
[5] O. Zatsarinny and S. S. Tayal, J. Phys. B **34**, 1299 (2001).
[6] O. Zatsarinny, Comput. Phys. Commun. **174**, 273 (2006).
[7] U. Fano, Phys. Rev. **124**, 1866 (1961).
[8] U. Fano and J. W. Cooper, Phys. Rev. **137**, A1364 (1965).
[9] C. Froese Fischer, Comput. Phys. Commun. **64**, 369 (1991).
[10] O. Zatsarinny and C. Froese Fischer, Comput. Phys. Commun. **124**, 247 (1999).
[11] S. S. Tayal, J. Phys. B **28**, 5193 (1995).
[12] S. S. Tayal and G. P. Gupta, Astrophys. J. **526**, 544 (1999).
[13] W. C. Martin, R. Zalubas, and A. Musgrove, J. Phys. Chem. Ref. Data **19**, 821 (1990).
[14] L. Johansson, C. E. Magnusson, I. Joelsson, and P. O. Zetterberg, Phys. Scr. **46**, 221 (1992).
[15] S. N. Nahar and A. K. Pradhan, J. Phys. B **26**, 1109 (1993).
[16] H. G. Berry, R. M. Schectman, I. Martinsen, W. S. Bickel, and S. J. Bashkin, J. Opt. Soc. Am. **60**, 335 (1970).
[17] D. J. G. Irwin, A. E. Livingston, and J. A. Kernahan, Nucl. Instrum. Methods 110, 111 (1973).
[18] A. E. Livingston, P. D. Dumont, Y. Baudinet-Robinet, H. P. Garnir, E. Biemont, and N. Grevesse, *Beam Foil Spectroscopy*, edited by I. A. Sellin and D. J. Pegg (Plenum, New York), p. 339.
[19] L. J. Ryan, L. A. Rayburn, and A. J. Cunningham, J. Quant. Spectrosc. Radiat. Transf. 42, 295 (1989).
[20] A. Hibbert, Comput. Phys. Commun. **9**, 141 (1975).
[21] P. C. Ojha and A. Hibbert, J. Phys. B **22**, 1153 (1989).
[22] C. A. Ramsbottom, K. L. Bell, and R. P. Stafford, At. Data Nucl. Data Tables **63**, 57 (1996).
[23] S. S. Tayal, Astrophys. J., Suppl. Ser. **111**, 459 (1997).
[24] L. Quigley and K. A. Berrington, J. Phys. B **29**, 4529 (1996).
[25] T. W. Gorczyca and N. R. Badnell, J. Phys. B **29**, L283 (1996).
[26] N. R. Badnell, T. W. Gorczyca, and A. D. Price, J. Phys. B **31**, L239 (1998).